Chemistry Europe
European Chemical Societies Publishing

WILEY VCH

Excellence in Chemistry Research

Announcing our new flagship journal

- Gold Open Access
- Publishing charges waived
- Preprints welcome
- Edited by active scientists

Meet the Editors of *ChemistryEurope*

Luisa De Cola
Università degli Studi di Milano Statale, Italy

Ive Hermans
University of Wisconsin-Madison, USA

Ken Tanaka
Tokyo Institute of Technology, Japan

Batteries & Supercaps

Research Article
doi.org/10.1002/batt.202300298

Chemistry Europe
European Chemical Societies Publishing

www.batteries-supercaps.org

Special Collection

Surface Properties-Performance Relationship of Aluminum Foil as Negative Electrode for Rechargeable Aluminum Batteries

Noha Sabi,*[a, b] Krishnaveni Palanisamy,[c] Fatemehsadat Rahide,[a] Sven Daboss,[c] Christine Kranz,[c] and Sonia Dsoke*[a]

Rechargeable aluminum batteries with aluminum metal as a negative electrode have attracted wide attention due to the aluminum abundance, its high theoretical capacity and stability under ambient conditions. Understanding and ultimately screening the impact of the initial surface properties of aluminum negative electrodes on the performance and lifetime of the battery cell are of great significance. The purity, surface finishing and degree of hardness of aluminum metal may strongly impact the device's performance, but these properties have not been systematically studied so far. Here, we present an investigation of the underestimated but crucial role of the aluminum foil surface properties on its electrochemical behavior in aluminum battery half-cells. The results show that commercial aluminum foils with the same purity and degree of hardness but with different thicknesses (from 0.025 to 0.1 mm) exhibit different microstructure and surface roughness, which in turn have an impact on the cyclability. Atomic force microscopy studies show that the aluminum foil is corroded after repeated electrochemical cycling, thus leading to cell failure. The sample with 0.075 mm thickness exhibits the best cycling stability.

Introduction

The ever-increasing demand for lithium-ion batteries (LIBs) have challenged scientists and engineers to seriously develop alternative electrochemical energy storage systems based on more abundant and natural resources. Lithium and cobalt which are the main LIBs components are not abundant and are located in geopolitically sensitive areas.[1]

Rechargeable aluminum batteries (RABs) using aluminum (Al) metal as the negative electrode material offers a high theoretical capacity due to the multivalent ions transfer and have been considered as one of the sustainable and future promising energy storage systems.[2–5]

Al is the most abundant metallic element in the earth's crust (82000 ppm);[6] nevertheless, Al is extracted from bauxite, and its production requires substantial energy, leading to high production costs that are sometimes not taken into account in the literature.[7–11] However, the Al recycling process is well developed and established, still making Al a very appealing metal.[12]

From an energy storage perspective, Al is able to transfer three electrons per atom, offering the highest gravimetric and volumetric capacities of 2980 mAh g^{-1} and 8046 mAh cm^{-3} (vs. 3861 mAh g^{-1} and 2042 mAh cm^{-3} for Li), respectively.[13] Compared to other metals used in batteries, Al is less reactive in air due to its high electronegativity (1.61 on the Pauling scale).[14]

Despite these advantages, the development of Al batteries faces several challenges related to the use of acidic ionic liquid (IL)-based electrolyte solutions, which are highly corrosive and make Al batteries sensitive to moisture. The commonly used IL-based electrolytes are obtained by mixing $AlCl_3$ salt with an imidazolium salt, bearing long-chain organic cations such as 1-ethyl-3-methylimidazolium (EMIm) or 1-butyl-3-methylimidazolium (BMIm) and halogen anions (Cl^-, Br^- or I^-).[15] The molar ratio between the $AlCl_3$ and the ionic liquid determines the amount of the $Al_2Cl_7^-$ "active" species being the key point for the plating/stripping performance. Efficient plating/stripping is observed for $AlCl_3$ mixed with EMImCl in a molar ratio higher than 1,[16,17] where the electrolyte contains $Al_2Cl_7^-$ (which reduces at the negative electrode side, giving rise to metallic Al) and $AlCl_4^-$, which intercalates in the positive carbon-based electrode material[18] (typically graphite).

[a] Prof. Dr. N. Sabi, F. Rahide, Prof. Dr. S. Dsoke
Institute for Applied Materials (IAM)
Karlsruhe Institute of Technology (KIT)
Hermann-von-Helmholtz-Platz 1, 76344 Eggenstein-Leopoldshafen (Germany)
E-mail: noha.sabi@um6p.ma
sonia.dsoke@kit.edu
Homepage: https://htmr.um6p.ma/
http://www.iam.kit.edu/ess/english/663.php

[b] Prof. Dr. N. Sabi
High Throughput Multidisciplinary Research (HTMR)
Mohammed VI Polytechnic University
Lot 660 Hay Moulay Rachid, Ben Guerir, 43150 (Morocco)

[c] K. Palanisamy, Dr. S. Daboss, Prof. Dr. C. Kranz
Institute of Analytical and Bioanalytical Chemistry
Ulm University
Albert-Einstein-Allee 11, 89081 Ulm (Germany)

Supporting information for this article is available on the WWW under https://doi.org/10.1002/batt.202300298

Special Collection This publication is part of a joint Special Collection dedicated to Post-Lithium Storage, featuring contributions published in Advanced Energy Materials, Batteries & Supercaps, and ChemSusChem.

Research Article
doi.org/10.1002/batt.202300298
Chemistry Europe
European Chemical Societies Publishing

Different positive electrode materials[19–21] have been investigated and they can be classified with respect to the mechanism of intercalation or conversion. The intercalation mechanism consists in the reversible intercalation of the Al^{3+} cations into a layered host, for example, in vanadium oxide,[22] in Mo_6S_8 chevrel phase,[23] in metal disulfides[24] or the intercalation of $AlCl_4^-$ anions into a carbon material[25–28] such as graphite[29] and graphene.[30] The conversion mechanism is reported mainly for aluminum-chalcogen batteries, such as aluminum-sulfur batteries, which undergo a transition process of elemental sulfur to a series of sulfides (S_n^{2-}) and polysulfides ($Al_2Cl_2S_n^-$) with the final conversion to Al_2S_3.[31] One drawback of Al batteries is the standard potential (−1.66 V vs. SHE) of Al with its higher value compared to Li, sodium (Na), magnesium (Mg) and potassium (K),[32–34] which results in a small output cell voltage. However, this problem could be mitigated by some approaches. For example, a bipolar cell design has been reported in the literature.[35,36]

The charging mechanism of an Al 'metal-battery' with graphite as the positive electrode is illustrated in Scheme 1. At the positive electrode side, the tetrachloroaluminate anions ($AlCl_4^-$, which also result from the dissolution reaction of Al metal) are transported through the separator and intercalate into non-occupied lattice sites of the graphite. At the negative electrode side, aluminum plating takes place. During discharge, the processes are inverted ($AlCl_4^-$ deintercalates from graphite and Al is stripped from the anode, regenerating $Al_2Cl_7^-$).

Unlike other alkali metals (e.g., Li and Na), Al suffers from self-consumption because of its high Young's modulus.[37] Consequently, over long-term cycling, Al can be peeled off from the foil surface, dissolve into the electrolyte solution and migrate through the separator to deposit on the counter electrode. The consumption of the Al foil may lead to electrolyte leakage and give rise to safety issues. It is also worth mentioning that due to the manufacturing process, the Al_2O_3 passivating layer on both sides of the foil (shiny and non-shiny) has different thicknesses and distribution.[38] This insulating passivation layer is responsible for the initial poor cycling performance of Al anodes, and it is the reason why acidic electrolytes are needed to partially dissolve the oxide layer and create plating/stripping sites on the surface. In this respect, acidic IL-based electrolyte compositions based on $AlCl_3$ and EMImCl significantly contribute to the activation of the surface and reversible Al plating/stripping.[39]

Choi et al.[40] have investigated the electrochemical performances of Al metal as a negative electrode material with both native and very thin aluminum oxide (Al_2O_3) layers. It is reported that a thin layer of Al_2O_3 protects the aluminum metal from corrosion resulting in high and stable capacity values.[40] In another study, Long et al. investigated the *in situ* formation of Al dendrites during battery operation. The authors claimed that the dendrites growth occurs right after the dissolution of the Al_2O_3 layer and a solid-electrolyte interphase forms.[41] They concluded that a porous Al could maintain stable capacities over many cycles. Hence, the morphological as well as the surface properties of the foil as negative electrode material should have a significant impact on the cell's operation.

Rolled Al products find applications, e.g., as current collectors in lithium and sodium-ion batteries, also as negative electrode material for LIBs[42,43] and recently as negative electrode material for RABs. Although purity is not crucial for application as current collector in LIBs or NBs, when used as a negative electrode in RABs, the Al purity, thickness and surface roughness are particularly important but rarely reported in the literature.[44,45] It should be noted that Al foils with the same purity but with different surface finishing or different thicknesses purchased from the same manufacturer may exhibit different microstructures. The surface finishing as a selectable

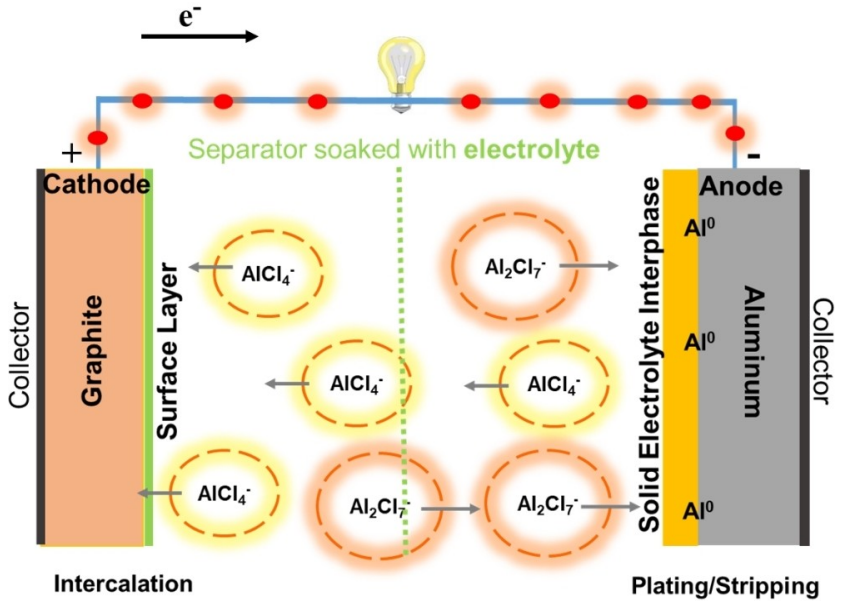

Scheme 1. Charging principle of an Al battery using graphite as intercalating positive electrode and Al metal as the negative electrode with $AlCl_3$/EMImCl as the electrolyte (molar ratio of 1.5/1).

Research Article
doi.org/10.1002/batt.202300298

parameter does not exist at most vendors and surface roughness parameters are usually not specified in data sheets.

During the fabrication of Al strips, rolling processes alternate with different annealing and abrasive cleaning processes (as illustrated in Scheme 2), directly influencing the surface properties. It is reported that the progression of the surface morphology of Al during cold-rolling is mainly determined by the surface in the "as-cast" state.[46] Due to physical and mechanical properties such as yield strength, hardness, electrical conductivity, bendability, or geometric dimensions such as thickness, Al can be manufactured via several processing routes, i.e., using two-high reversing mills or cluster mills, abrasive brushes including chemicals in the cleaning steps. Moreover, due to mechanical stress during rolling and brushing in cleaning processes, the surface can be strongly deformed resulting in the destruction of the initial grain composition. Depending on the production sequence and production parameters, fragmented layers can be formed, which impede subsequent coating of the metal surface, e.g., via electrochemical plating. Moreover, thin commercially available foils have two different sides due to two-layer rolling. The reasons for single-layer or two-layer rolling depend on the rolling mill, tensile strength, thickness and alloy, as well as company-relevant parameters cost, time and capacity. Technically, the thinnest foils which are rolled in a single layer are about 50 μm; however, mainly for cost reasons, two-layer rolling is often performed with thicknesses starting at 100 μm or even higher. For thick foils, the surface usually resembles the polished rolling surface (Scheme 2, left picture) in contrast to two-layer rolled foils, where only one side is affected by the polished rolling surface, whereas the surface properties of the other side are mainly affected by a second foil. Motivated by such differences arising from the production process, we believe that it is highly relevant to understand the impact of the choice of foils with the particular surface finish on the electrochemical performance (i.e., plating/stripping, efficiency and cycling stability).

Therefore, we used a combination of different analytical techniques, such as atomic force microscopy (AFM), scanning electron microscopy (SEM) and X-ray diffraction (XRD), to investigate Al foils with the same purity and degree of hardness but different thickness and correlate the properties to the electrochemical performance. With this study, we uncover how all these parameters are essential for the stability of the foil upon long-term cycling under accelerated aging conditions in $AlCl_3$/EMImCl (1.5 : 1) electrolyte.

Results and Discussion

Microstructural characterization of Al foils

The surface finishing of the pristine foils was imaged using microscopic techniques (AFM and SEM). For the sake of simplicity, in this paper, we refer to the foils as Al*x* (with $x = 0.1$, 0.075, 0.06, 0.05, 0.04 and 0.025, corresponding to the thickness in mm). The samples were measured as received without any prior surface cleaning or etching. AFM images (Figure 1) were taken at three different areas of each sample (Al0.1, Al0.075, Al0.06, Al0.05, Al0.04 and Al 0.025).

The SEM images depicted in Figure 2 reveal the microstructure of the pristine foils. For each foil, SEM images were taken at three different spots, providing coherent results. The different surface microstructure is clearly visible, and the SEM images agree with the AFM topography images shown in Figure 1. The Al0.1 and Al0.075 foils reflect rolling artifacts in one direction with random spacing and visible defects. For the Al0.06, Al0.05, Al0.04 and Al0.025 samples, the rolling stripes appear to be less pronounced with grain boundaries. Zoomed views also show stripes but with narrow spacing and with random oriented domains (see e.g., 0.06 but also 0.025). These observations are in agreement with the AFM results presented in Figure 1. As the foils come from the same manufacturer and

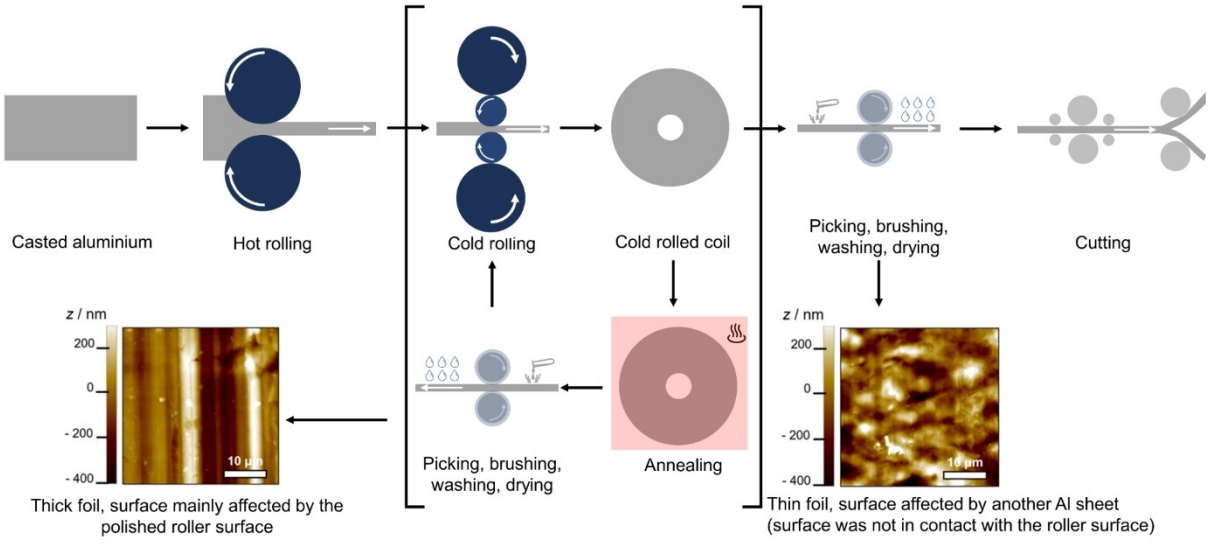

Scheme 2. Simplified scheme of the main manufacturing processes of rolled aluminum and how the process can affect its surface finishing.

Research Article
doi.org/10.1002/batt.202300298
Chemistry Europe
European Chemical Societies Publishing

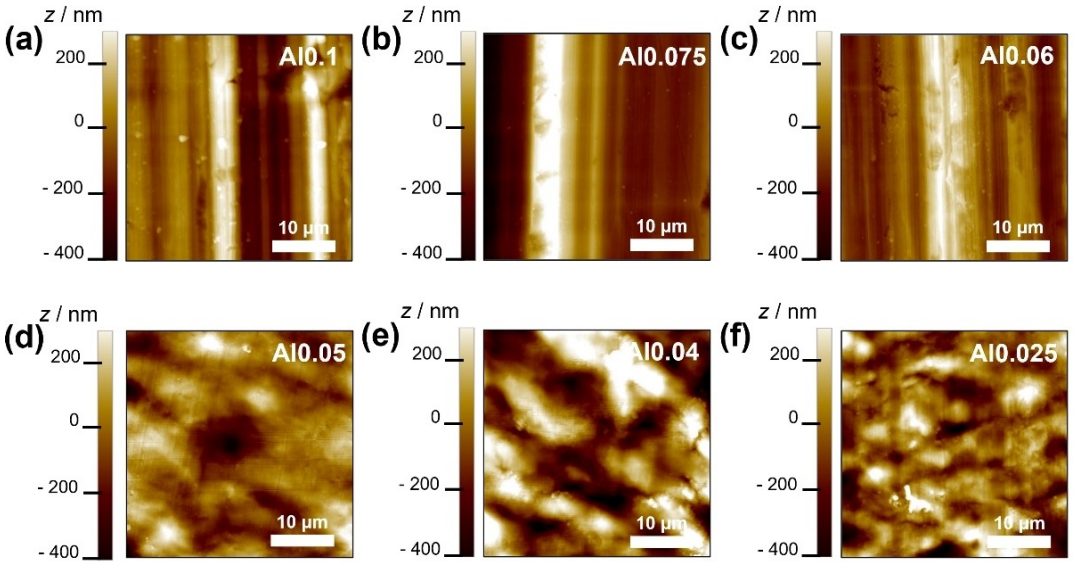

Figure 1. AFM topography images of the different pristine Al foils.

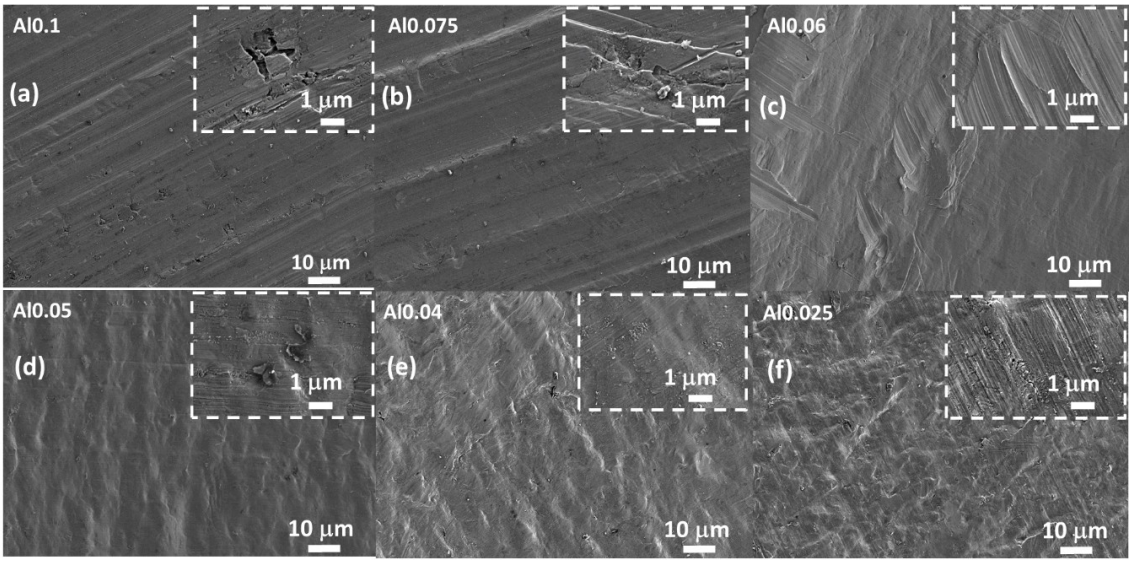

Figure 2. SEM images of the different pristine Al foils.

have the same purity, the different morphology should be correlated only to the rolling process applied to reach the required thickness during manufacturing. The XRD patterns of the different samples are depicted in Figure S2. The Al foils show the same sharp reflections 111, 200, 220 and 311 characteristic of the cubic close-packed structure with the space group Fm-3 m. Interestingly, the ratio between the main reflections 111 and 200 is not the same: $I_{200/111} = 0.62$; 1.125; 0.41; 0.214; 0.37; 0.521 for Al0.1, Al0.075, Al0.06, Al0.05, Al0.04, Al0.025, respectively. This difference in intensities indicates that the as-received foils do not exhibit the same microstructure. For the Al0.075, the 200 reflection is exceptionally intense in comparison to the 111 reflection. This difference impacts the stability upon electrochemical cycling, as we will explain later. Overall, the results obtained from SEM, XRD and AFM confirm that the structure and surface properties of the Al foils vary depending on the manufacturing process regardless of the purity.

Electrochemical characterization via cyclic voltammetry

Figure 3(a–f) shows the cyclic voltammograms of the Al foils recorded at a scan rate of 10 mV/s in the voltage range of −0.5–2 V vs. Al. The CV curves look similar independently of the Al foil. Except for the Al0.075 sample, the first CV scan shows almost zero current density, probably due to the Al_2O_3 layer initially present on the foil surface, which hinders the pathways for the ionic species.[41] Starting from the 5th cycle, the plating/stripping current densities sharply increase, indicating the

Research Article
doi.org/10.1002/batt.202300298
Chemistry Europe
European Chemical Societies Publishing

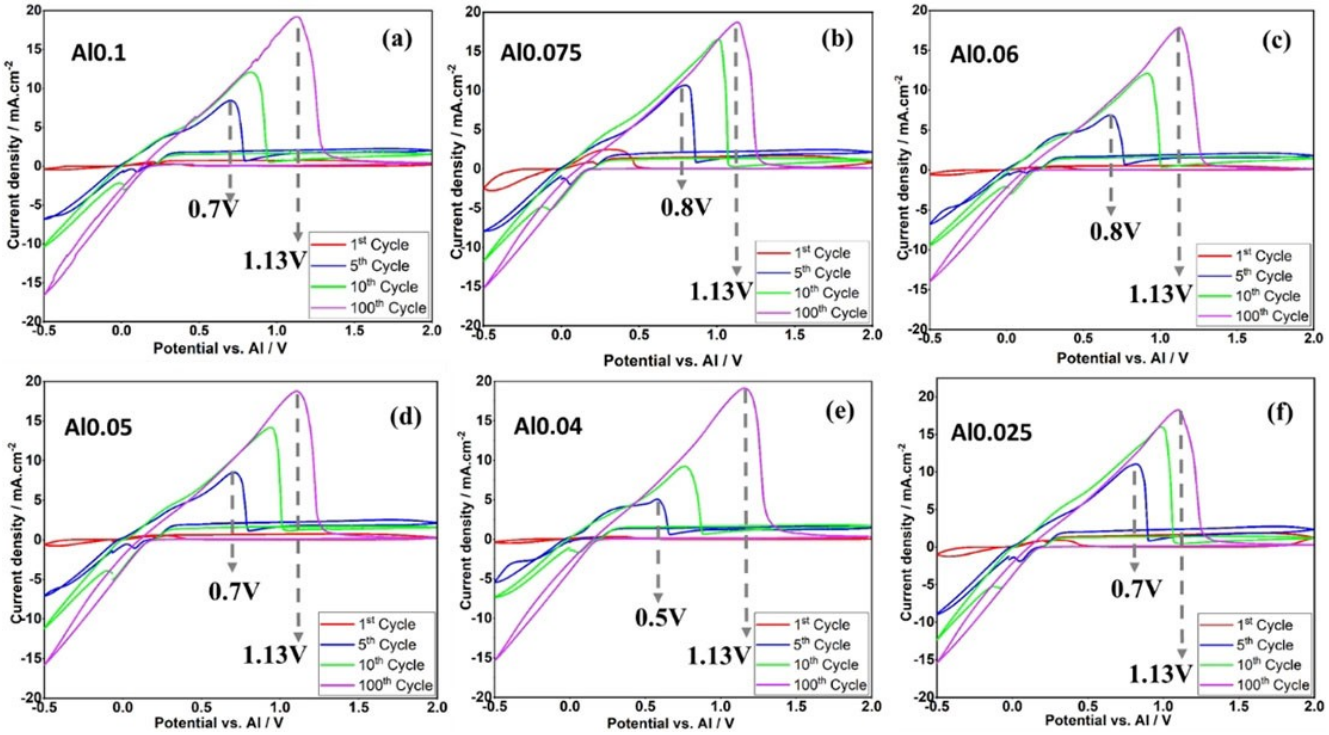

Figure 3. CV curves of Al foils at 10 mV/s: a) Al0.1, b) Al 0.075, c) Al 0.06, d) Al 0.05, e) Al 0.04 and f) Al 0.025 recorded in $AlCl_3$/EMImCl (1.5/1) at 10 mV/s.

progressive dissolution of the passivation layer, as also reported by other authors.[42] In addition, from the 5th cycle, a sharp oxidation peak appears during the anodic scan in the potential region of 0.5–0.7 V vs. Al for all foils. The oxidation peak gradually shifts to around 1.1 V vs. Al, broadens and increases in intensity over 100 cycles. This could be due to the onset of corrosion of the Al foil and an increase in polarization, which will be discussed later. The plating/stripping capacities and the coulombic efficiencies of the foils are compared in Figure 4. The first observation is that the stripping capacities are two times higher than the plating capacities (from the 1st to the 10th cycle, the coulombic efficiency is lower than 56%). Moreover, both plating and stripping capacities are not stable and increase dramatically from the 1st cycle until the 20th–30th cycles, when they stabilize. This confirms our first assumption about the role of the passivation layer initially present on the Al foil surfaces and indicates how much time is required to activate the sites for Al plating and stripping. The enlarged areas of the plating, stripping capacities and coulombic efficiency graphs from the 30th to 100th cycles presented in Figure 4(a–c) clearly indicate that the Al0.075 shows stable capacities and good coulombic efficiency. The unstable plating capacity (fluctuations in coulombic efficiency as observed for the Al0.1 and Al0.04 in the zoomed view of Figure 4a–c) suggests random electrodeposition of Al on the surface and inevitable formation of dendrites. After 80 cycles, the coulombic efficiency stabilizes at around 85% for all foils except for Al0.04.

Figure 5(a–c) presents the cycling performances of the different foils at the higher scan rate of 20 mV/s. All samples show a similar plating/stripping trend: the capacities drastically increase until reaching their maximum at the 100th cycle; after that, they decrease slightly and stabilize until the 300th cycle. Similar to what was observed at 10 mV/s, the stripping capacities are higher in comparison to the plating capacities. However, more differences in plating/stripping capacities among the foils are observed when the scan rate is increased to 20 mV/s. Al0.075 shows the highest capacities, followed by the Al0.06. The distinct differences in the foils' performances observed at 20 mV/s could be explained by deposition, which could lead to different deposition morphologies and uneven distribution of the dendrites. From the results obtained above, we could claim that the stable cycling performance (stable capacity for 100 cycles) observed for the Al0.75 is related to its initial microstructure (this foil shows a dominant crystal orientation at 200, unlike the other foils).

Ex-situ characterization of the aluminum foils

AFM experiments of the cycled foils were carried out to visualize the changes in surface morphology after recording 10 and 100 cyclic voltammograms at 10 mV/s (Figure 6), respectively. (The Al0.04 foil was excluded for this experiment in order to reduce the samples number).

After 10 cycles, all Al foils show an altered morphology, independently of the initial surface finishing. After only 10 cycles, the Al0.025 and Al0.05 samples (Figure 6e and d) show granular features, which can be ascribed to the random deposition of Al metal. The granular structure is more evident in the case of Al0.025. On the other hand, after 10 cycles, Al0.06

Research Article
doi.org/10.1002/batt.202300298
Chemistry Europe
European Chemical Societies Publishing

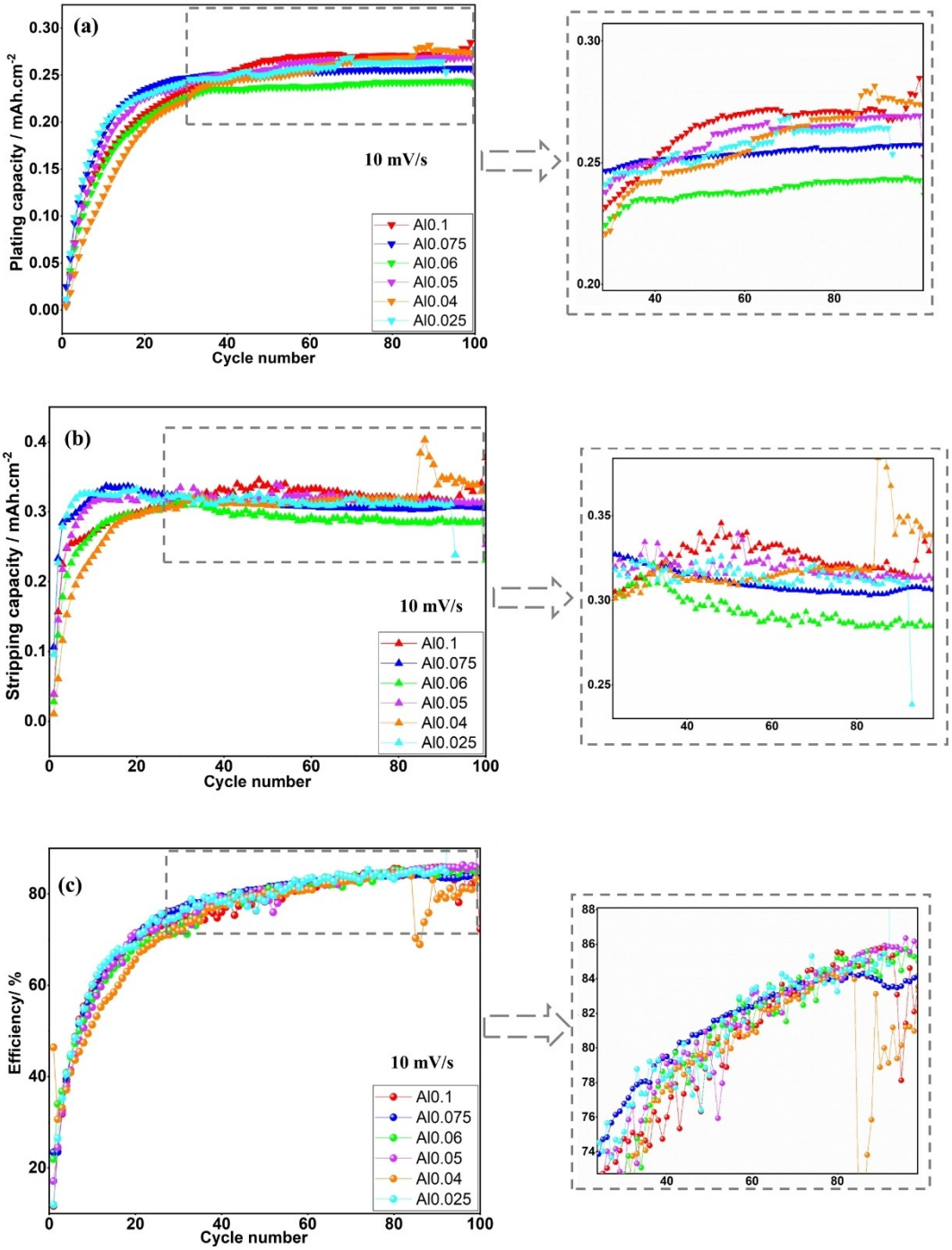

Figure 4. Cycle life of the Al foils. a) Plating capacity, b) stripping capacity and c) coulombic efficiency at 10 mV/s.

and Al0.1 show cracks/fractures, which could be explained by the severe volume changes upon plating and stripping. Surprisingly, Al0.075 shows the least cracked/fracture microstructure, which we attribute to a more homogeneous Al deposition.

After 100 cycles, all samples show the granular microstructure (Figure 6f–j), which is expected due to the Al deposition. From the above results, the change in the surface of the foils after cycling does not follow a specific trend related to the thickness. This change is instead related to the surface roughness and microstructure resulting from the manufacturing process. For example, the Al0.025 sample exhibits (as revealed by AFM and SEM images) a rough surface with many grain boundaries, which are thermodynamically unstable sites for dendrites growth, resulting in non-homogeneous Al deposition. The foil oriented at 200 shows the most stable electrochemical performance, which could be because this orientation is less prone to the dendrite's formation. This could be explained by

Research Article
doi.org/10.1002/batt.202300298
Chemistry Europe
European Chemical Societies Publishing

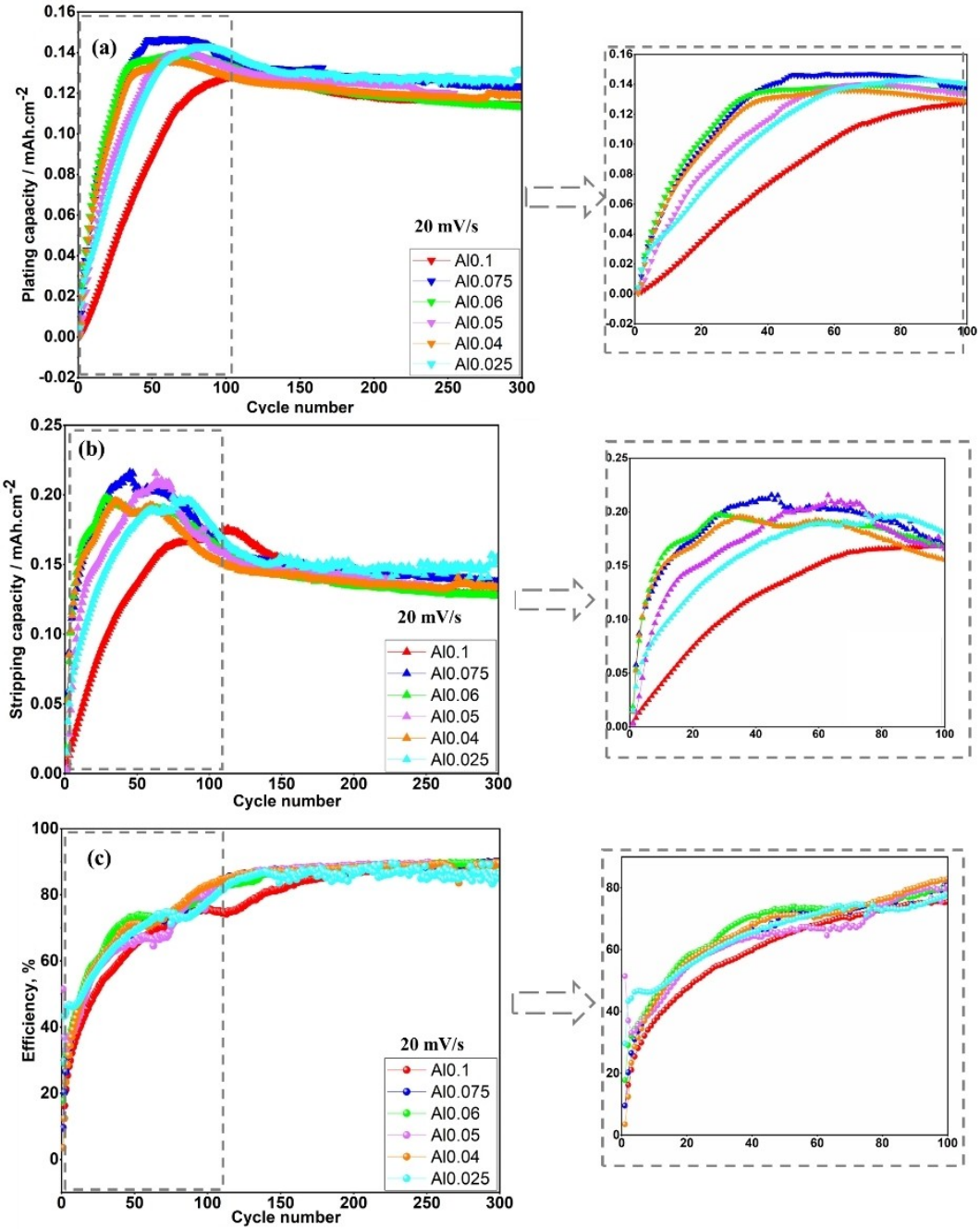

Figure 5. Cycle life of the different Al foils in $AlCl_3$/EMImCl (1.5/1). a) Discharge capacity, b) charge capacity and c) coulombic efficiency at 20 mV/s.

the fact that the 200 has low energy barrier for Al plating and stripping.[47]

In fact, upon electrochemical cycling, Al is randomly deposited upon plating, leading to dendrite formation and growth along specific orientations (which is confirmed by *ex-situ* XRD). At the same time, the surface roughness increases due to Al deposition and the surface shows corrosion pits. To some extent, after extensive plating and stripping and due to the large amount of electrolyte used (800 μL), the dendrites are dissolved in the acidic electrolyte leading to the generation of a new surface manifested by decreased surface roughness. The severe corrosion observed after 100 cycles is in agreement with the shifts of the anodic peaks in the cyclic voltammograms presented in Figure 3. After 100 cycles, the surface of all foils dramatically changes from a smooth appearance (SEM images in Figure 2) to defined particles at the surface (SEM images in Figure 7). Figure 7 shows that after 100 CV cycles, the surface exhibits a distribution of round agglomerated particles with two features: a growth of dense particles and corrosion pits. The Al0.075, Al0.025, and 0.1 samples have more agglomerated particles than the other samples. By combining the AFM and SEM results, we can conclude that the Al0.025 is more

Research Article
doi.org/10.1002/batt.202300298
Chemistry Europe
European Chemical Societies Publishing

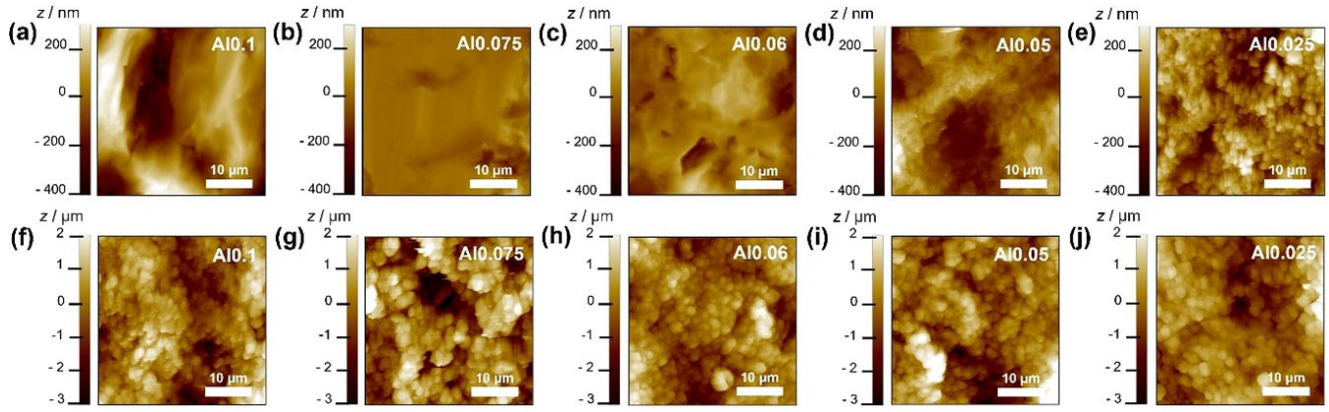

Figure 6. AFM topography images (30×30 µm) of Al foils. a–e) Al foils cycled 10× and f–j) Al foils cycled 100× (in $AlCl_3$/EMImCl electrolyte).

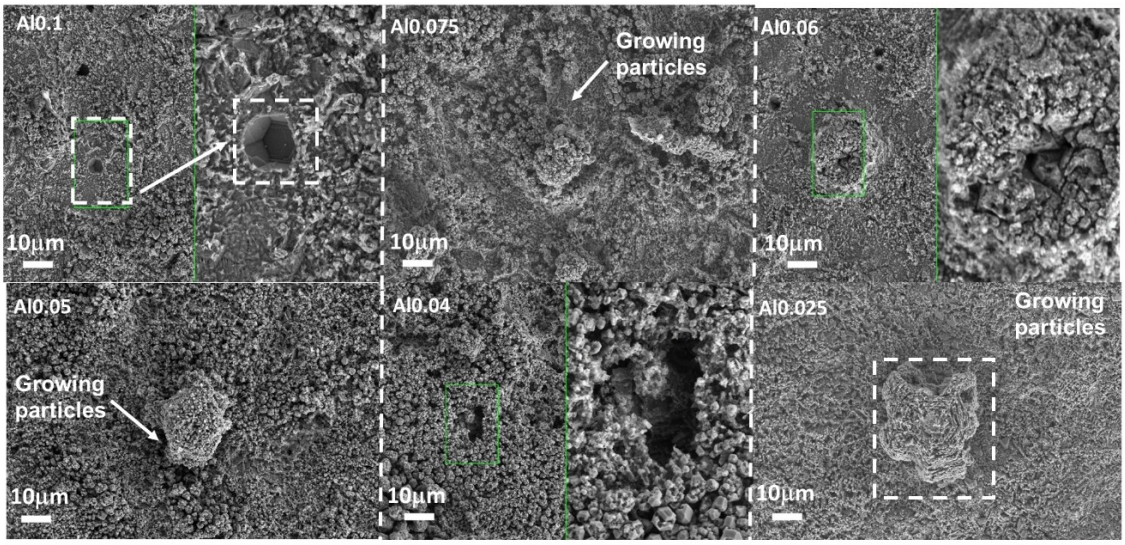

Figure 7. SEM images of Al foils after 100 CV cycles in $AlCl_3$/EMImCl (1.5/1).

susceptible to dissolution upon electrochemical cycling and in contact with the IL-based electrolyte due to the instability of the deposited Al. This is mainly due to the presence of grain boundaries and the likely dendrites formation along the 111 directions. Due to the low energy barrier, dendrites tend to form according to the closed-packed plan as claimed in literature[47] After 100 cycles, the Al0.025 foil surface becomes smoother with agglomerated particles confirming the formation of a new surface.

As the Al foils initially exhibit different microstructures and surface roughness, it is important to evaluate the plating/stripping mechanism at the surface of each foil after 100 cycles. Figure S4 shows the XRD patterns of the foils after 100 cycles compared to the pristine ones. For all foils, we focused on the dominant reflections, which are 111 and 200. It is observed that the intensity of the 111 reflection decreases slightly for the Al0.1 and Al0.75 and drastically for the other foils (after 100 cycles). This decrease is more pronounced for Al0.025, which explains the generation of a new surface revealed by AFM results.

Accelerated aging by cycling at high temperature

Considering the AFM and SEM images collected after 100 cycles at room temperature, it is evident that the Al foil can be dissolved and consumed upon electrochemical cycling. To get more insights into the stability of the foils, we conducted cyclic voltammetry at 60 °C and 80 °C (Figures 8 and 9), respectively.

At the first cycle, the plating/stripping current densities are higher in comparison to what is obtained at room temperature. Obviously, the density and viscosity of the IL-based electrolyte decrease at high temperatures, improving the mobility of ions.[39] In addition, the high temperature could facilitate the dissolution of the native Al_2O_3 layer. However, after 12 cycles, the Al0.025 electrode is destroyed, as shown in the inset of Figure 8(f). The Al0.04 and Al0.05 samples deteriorate com-

Research Article
doi.org/10.1002/batt.202300298
Chemistry Europe
European Chemical Societies Publishing

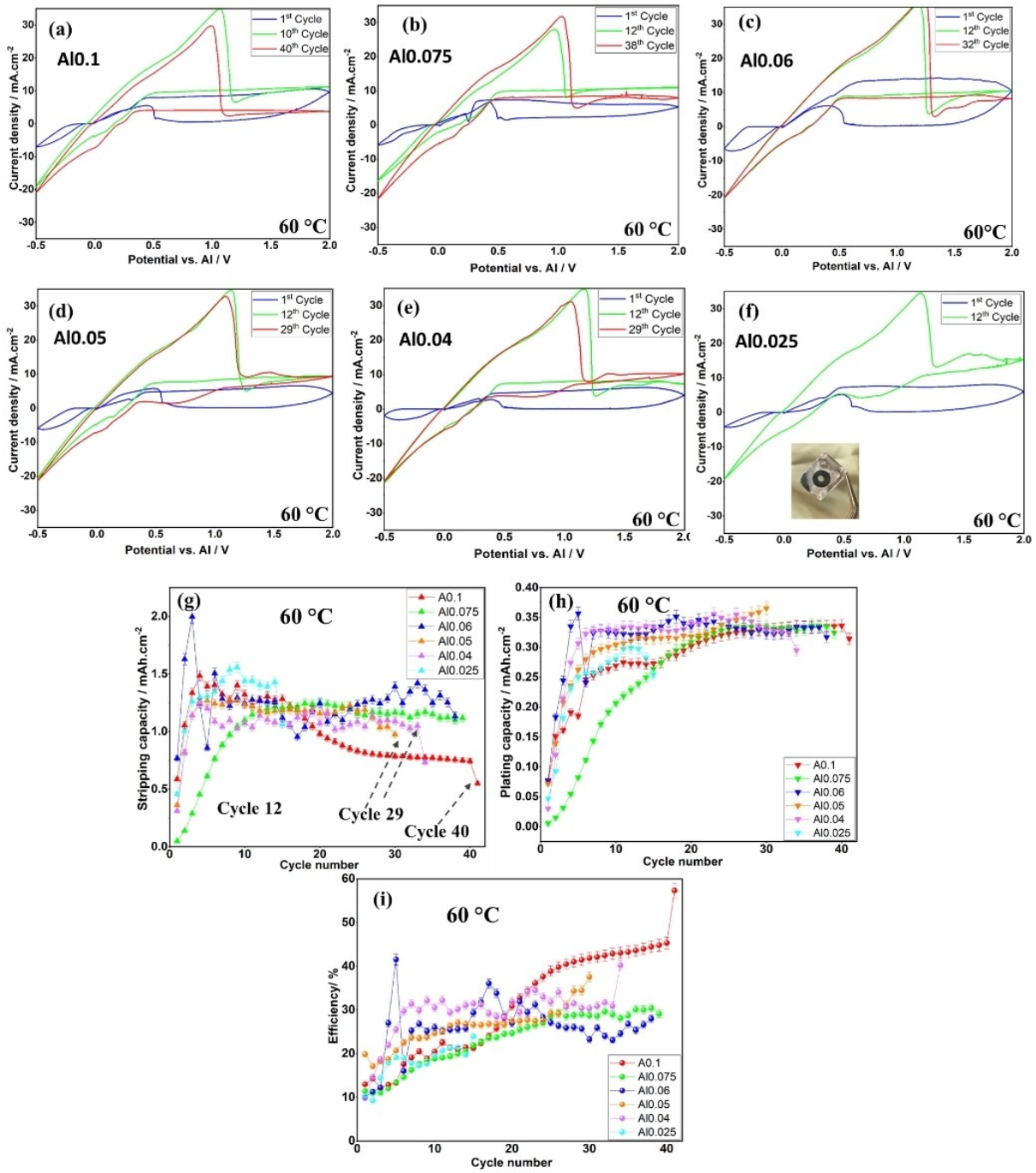

Figure 8. CV curves of: a) Al0.1, b) Al0.075, c) Al 006, d) Al0.05, e) Al0.04 and f) Al0.025 at 10 mV/s at 60 °C. Comparison of the g) plating capacities, h) stripping capacities and i) efficiencies of the different foils at 60 °C with error bars.

pletely after 28 cycles, which is indicated by an oxidation peak at around 1.4 V. This peak corresponds to the oxidation of the gold-plated thermo block of the TSC surface cell (shown in Figure S1), which is exposed to the electrolyte after the complete corrosion of the Al sample. Finally, the Al 0.06, Al0.075 and Al0.1 foils could withstand until 32nd, 38th and 40th cycles, respectively.

Figure 8(g and h) shows the plating/stripping capacities of the different foils at 60 °C. As also observed in the room temperature experiments, the capacities in stripping are higher than in plating, resulting in low coulombic efficiency (Figure 8i). This result shows that the aluminum removed during oxidation is not deposited back on the surface and it is either in the electrolyte solution or deposited on the glassy carbon counter electrode surface.

The coulombic efficiency, observed for all foils, is initially extremely low (around 10 %) and increases to around 25 % after 10 cycles. However, the values are not stable, as shown in

Research Article
doi.org/10.1002/batt.202300298
Chemistry Europe
European Chemical Societies Publishing

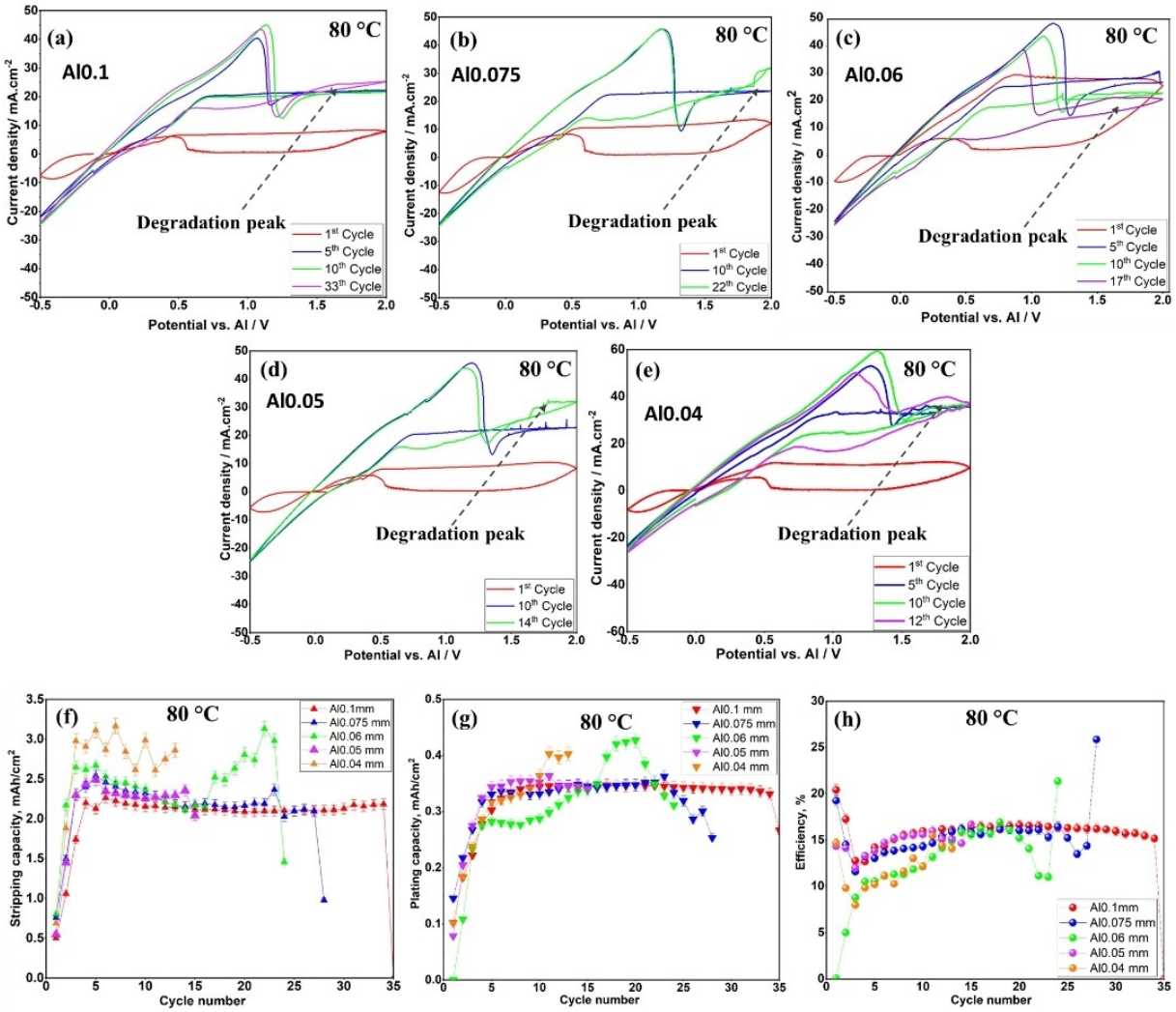

Figure 9. CV curves of: a) Al0.1, b) Al0.075, c) Al0.06, d) Al0.05 and e) Al 0.04 and at 10 mV/s at 80 °C. Comparison of the f) plating capacities, g) stripping capacities and h) coulombic efficiencies of the different foils at 80 °C with error bars.

Figure 8(i). The highest efficiency is observed for Al 0.1, but still, it does not exceed 50 %.

Increasing the temperature to 80 °C enhances the plating/stripping capacities (Figure 9), but unfortunately, the degradation process is also accelerated, as the foils can only withstand a few cycles; the maximum is 33 cycles for the Al0.1. The Al0.04, Al0.05, Al0.06 and Al0.075 are destroyed after 12th, 14th, 17th and 22nd cycle, respectively. Due to its inferior durability at 60 °C, the Al0.025 foil was not tested at 80 °C. The foils exhibit an initial coulombic efficiency of only 15 to 20 % at this temperature.

The first cycle recorded at 25 °C, 60 °C and 80 °C for each foil are compared in Figure S3, to demonstrate how the temperature enhances the plating/stripping current densities. After the first stripping process, the current increases continuously together with the anodic polarization; a steady/constant current evolution is observed between 2 and 0.4 V where it decreases again until the plating potential. The same trend is observed for the following cycles (see Figures 8 and 9). The observed behavior correlates with the foil deterioration after a few cycles. Strong oxidation (corrosion) of the aluminum, regardless of the thickness or surface finishing, occurs due to the increased temperature.

These experiments demonstrate that increasing the temperature enhances the stripping process with quick Al consumption during the anodic scan.

Effect of the electrolyte/electrode contact on the foils' microstructure

In order to investigate whether the microstructure of the films is mainly affected by the contact with the acidic electrolyte or by the stress induced during the electrochemical experiments, the following tests were carried out: The effect of the contact with the electrolyte was investigated separately by immersing the foils for the same time needed to perform 10 (6 hours) and 100 (18 hours) cycles at 10 mV/s. Al0.025 and Al0.075 showed the lowest and highest cycling stability, respectively, so they were used for the contact tests. The foils were immersed for 6 hours and 18 hours in the electrolyte without applying a bias.

Research Article
doi.org/10.1002/batt.202300298
Chemistry Europe
European Chemical Societies Publishing

After immersion, the surface morphology of the Al foils was again evaluated by AFM, and the results are depicted in Figure 10. The surface morphology of Al0.025 samples exposed to the electrolyte for 6 h and 18 h shows only minor changes that are within the statistical uncertainty of the measurements. Al0.025 shows no statistically significant difference in roughness, while Al0.075 shows a decrease in surface roughness with increasing immersion time. The bar graph of mean Sa values for both foils is shown in Figure S5 (Supporting Information). Comparing these results with the AFM results shown in Figure 6, it is evident that the surface roughness of all foils increases dramatically after cycling. However, immersing the foils for 6 and 18 hours leads to a slight decrease in surface roughness. These opposite behaviors lead to two assumptions:

(1) under dynamic conditions: the increase of surface roughness during cycling can be explained by corrosion and the inhomogeneous aluminum deposition on the negative electrode in the IL-based electrolyte.
(2) under static conditions: the decrease of the surface roughness upon immersion in the IL-based electrolyte is probably due to the partial dissolution of the native Al_2O_3 layer and the change in the microstructure with a formation of a smooth new passivation layer.[48]

The microstructure of the immersed foils was also evaluated by SEM and the results are presented in Figure 11. In the case of Al0.025, the surface slightly changes after exposure to the electrolyte for 6 and 18 hours. This result is consistent with the decrease in surface roughness observed by AFM. After 18 h

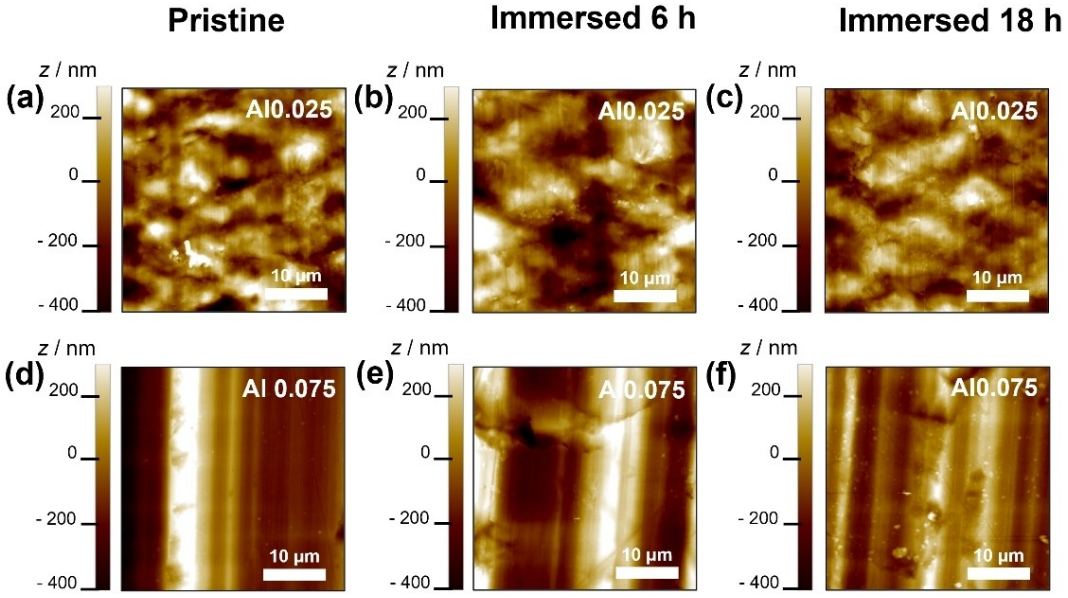

Figure 10. AFM images (30×30 µm) of: a) Al0.025 (pristine), b) Al0.025 6 h, and c) Al0.025 18 h immersion time in $AlCl_3$/EMImCl electrolyte. d) Al0.075 (pristine), e) Al0.075 6 h and f) 18 h immersion time in $AlCl_3$/EMImCl electrolyte.

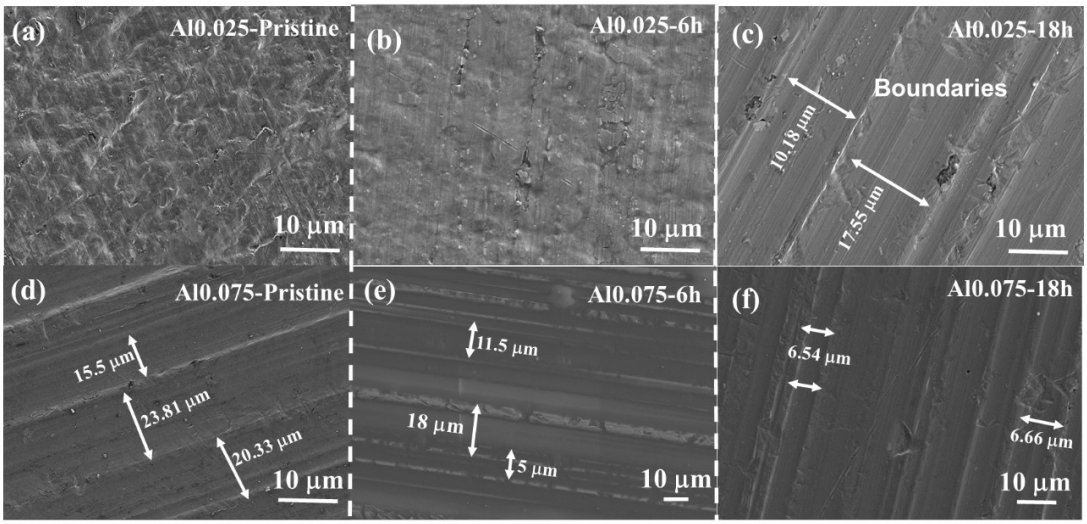

Figure 11. SEM images of the Al0.075 and Al0.025, a and d) as received, b and e) 6 h immersed, c and f) 18 h immersed in $AlCl_3$/EMImCl (1.5/1), respectively.

Research Article
doi.org/10.1002/batt.202300298
Chemistry Europe
European Chemical Societies Publishing

immersion, some clear strips (separated by 10.18 and 17.55 μm) with corrosion pits are visible. On the other hand, after 6 h and 18 h immersion of the Al0.075 foil in the electrolyte, the rolling features (stripes) appear slightly more pronounced but have the same appearance in terms of orientation.

To check whether the immersion of foils affects the crystallographic orientations of the aluminum, we analyzed the structure of the samples after 6 and 18 hours of immersion into the IL-based electrolyte. Figure 12(a and c) show the XRD patterns of the Al0.025 and Al0.075 as received and immersed in the IL-based electrolyte. The normalized integrated intensity, P_{hkl}, for the 111, 200, 220, 311 and 222 reflections are calculated following Equation (1):[49,50]

$$P_{hkl} = (I_{hkl}/(\sum I_{hkl}))/(Ir_{hkl}/(\sum Ir_{hkl})) \quad (1)$$

where I_{hkl} is the peak intensity of the (*hkl*) reflection of the samples; ΣI_{hkl} is the sum of peak intensities of the samples; Ir_{hkl} is the peak intensity of the (*hkl*) reflection obtained from the ICSD database[51] and ΣIr_{hkl} is the sum of peak intensities. The crystallographic orientations are presented in Figure 12(b and d).

Comparing the variation of the crystallographic orientations for the Al0.025 and Al0.075 foils after different immersion time in the IL-based electrolyte, it appears that the 0.025 foil shows more changes in the crystallographic orientations.

For the Al0.025, the corresponding 111 and 220 reflections increase their intensities after 6 h immersion into the electrolyte. After 18 h immersion, the 111 decreases its intensity and the 200 increase it. This suggests that the 200 reflection is more affected by the immersion time. After 6 h, the reflection intensity decreases slightly and then increases dramatically after 18 h. For the Al0.075, all reflections increase slightly after 6 h of immersion and decrease after 18 h of immersion. From the combined XRD, AFM and SEM results, it can be concluded that Al0.025, with its initial surface properties/microstructure, is more sensitive to the immersion time when in contact with the $AlCl_3$/EMImCl electrolyte.

In fact, the as-received foils, regardless of the thickness, exhibit different surface properties due to the manufacturing process. Two main features have a strong influence on the electrochemical performance, and these are surface microstructure and surface roughness (grain boundaries).[52] The lower the surface roughness (fewer grain boundaries), the better the electrochemical performance. The Al0.025 specifically has shown instability and drastic change in the microstructure after electrochemical plating/stripping and slight changes after immersion into the acidic electrolyte, which leads to faster deterioration. Dramatic changes in the microstructure are observed for the Al0.05 and Al0.06 foils as well. We can conclude that due to the presence of grain boundaries, the surface of these foils is thermodynamically unstable and prone

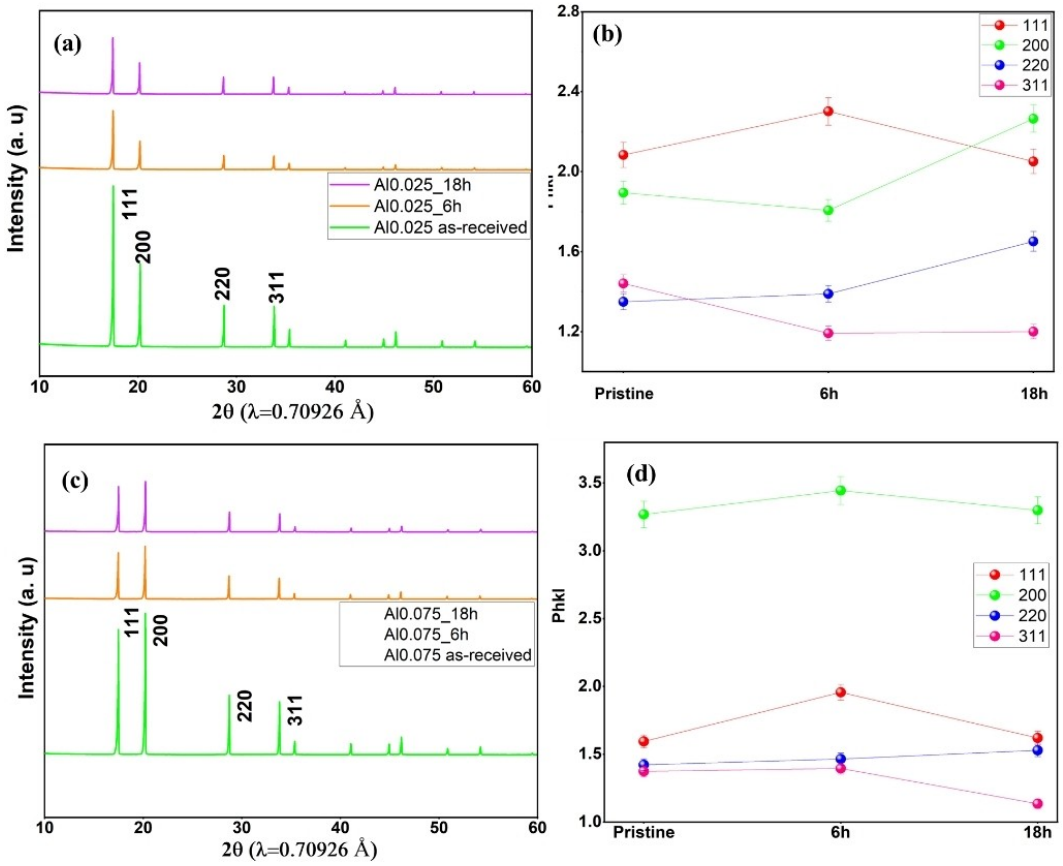

Figure 12. XRD pattern of the as-received foils, immersed for 6 and 18 h in $AlCl_3$/EMImCl. a) Al0.025 and c) Al0.075. Corresponding normalized peak intensity, P_{hkl}, from XRD reflections b) Al0.025, d) Al0.075 with error bars.

to change the microstructure even when just in contact with the acidic electrolyte.

Conclusions

In summary, we have investigated the effect of aluminium foil surface properties (of commercial Al foils of identical purity and from the same manufacturer) on the electrochemical properties in an $AlCl_3$/EMImCl IL-based electrolyte.

This comparison of the foils seems trivial, but it plays a vital role in determining the electrochemical performances of the Al-half cell and is also important when comparing data presented in the literature. In fact, the surface of the foils is strongly dependent on the rolling process applied during manufacturing, which results in different surface finishing. AFM measurements reveal different surface roughness of the as-received foils. The foils with the highest surface roughness (Al0.025 and Al0.05) are unstable upon electrochemical cycling and are quickly deteriorated, leading to safety issues (i.e., complete consumption of the foil in some points and, consequently, electrolyte leakage). The XRD diffractograms reveal different microstructures of the as-received foils. The *ex situ* investigations align with the electrochemical data, showing that the Al0.075 foil has the best cycling performances due to its low surface roughness and preferred orientation (200), which is less prone to dendrites growth. In conclusion, three important parameters should be considered when selecting an Al foil: (1) the surface roughness (as a rough surface with grain boundaries induces an unstable and random Al deposition), (2) the crystal orientation (some crystal orientations are prone to dendrites growth) and (3) the foil thickness (due to the irreversible consumption of the foil during long term cycling).

Experimental Section

Materials and chemicals

Electrolyte preparation

The preparation and handling of the IL-based electrolyte were conducted in an argon-filled glovebox (MBraun, O_2, $H_2O < 0.5$ ppm). The preparation consists of a slow adding of $AlCl_3$ (anhydrous, Sigma Aldrich, 99,99%) to EMImCl (Sigma Aldrich, $> = 95\%$) at a molar ratio of 1.5/1 ($AlCl_3$/EMImCl) while stirring using a magnetic bar at room temperature.[53] The final solution is a yellowish viscous liquid.

1) Al negative electrode
2) The Al foils were purchased from Goodfellow (purity: 99%, temper: annealed) with different thicknesses: 0.025 mm, 0.04 mm, 0.05 mm, 0.06 mm, 0.075 mm and 0.1 mm. Preparation of *ex situ* samples (Al negative electrodes after cycling)

After 10 and 100 cycles, the cells were disassembled inside the glovebox. The excess of electrolyte in the electrodes was removed by soaking/rinsing each foil three times with acetonitrile (anhydrous, Sigma Aldrich, 99,8%). Then, the foils were dried for one hour in the glovebox under vacuum to remove any residues of acetonitrile.

Characterization of the pristine and cycled Al foils

X-ray diffraction (XRD) measurements of the aluminum foils were performed with a STOE STADI P diffractometer (Germany) operated with Mo–Kα1 radiation ($\lambda = 0.7093$ Å) in rotating transmission mode. The Al foil was covered with a kapton film under argon.

The microstructure of the Al foils were studied with a Zeiss Supra 55 Scanning Electron Microscope (SEM) with a primary electron beam voltage of 15 keV. The samples were fixed on a steel sample holder by using carbon sticky tape.

All AFM measurements on the pristine and cycled Al foils were performed with an AFM microscope (Park NX10, Park Systems) located in a glovebox in an Ar atmosphere (MBraun, O_2, $H_2O <$ 0.1 ppm). Morphological changes and roughness of pristine and cycled Al foils were characterized using a closed loop scanner in non-contact mode and were measured before and after 10 and 100 cycles in $AlCl_3$/EMImCl electrolyte with the following thicknesses of the Al foils: 0.1, 0.075, 0.06, 0.05, 0.04 and 0.025 mm. Experiments were performed with high aspect ratio silicon AFM probes (PPP-NCHR, NanoWorld AG) with a resonant frequency of 330 kHz and a tip radius of 10 nm. Images were recorded at a scan speed of 0.7 Hz. The force constant of the cantilevers ($k = 42$ N/m) was determined using the thermal noise method.[54] Roughness data (Sa, arithmetic roughness) were analysed using Park's imaging processing tool for SPM data (XEI 5.2, Park Systems) from three different spots (30×30 μm, $n = 3$).

Two-tailed nonparametric Mann-Whitney U tests for data that are not normally distributed were performed. A significance level of $p = 0.05$ was selected. For the 0.025 mm Al foils at the $p = 00.05$ level, no statistically significant difference was determined, whereas for the 0.075 mm Al foils the difference proved to be statistically significant.

Electrochemical measurements

The electrochemical tests of the assembled cells were carried out with a Biologic potentiostat/galvanostat (Biologic VMP13) at a temperature of 25 °C, 60 °C and 80 °C in a voltage range of 0.5–2.0 V (vs. Al) at a scan rate of 10 mV/s or 20 mV/s, respectively. High scan rates are used because it has already been reported that the performance of the Al/graphite system is comparable to that of electrochemical supercapacitors in terms of power density.[55] As a matter of example, the cyclic voltammetry curves of the Al0.025 at 1 and 5 $mV\,s^{-1}$ are presented in Figure S6. The cyclic voltammetry tests were conducted in the TSC surface cell from rhd instruments (Germany) as a three electrodes airtight system shown in Figure S1 in the Supporting Information.

Acknowledgements

The authors acknowledge the support from RhD Intruments Company, Dr. Sebastian Kranz and Dr. Marcel Drüschler for the scientific discussions. The authors would like to thank Bettina Hunzinger for the SEM characterizations and Dr. Angelina Sarapulova for the scientific discussions. This work contributes to the research performed at CELEST (Center for Electrochemical Energy Storage Ulm-Karlsruhe) and was funded by the German Research Foundation (DFG) under Project ID 390874152 (POLiS Cluster of Excellence). Open Access funding enabled and organized by Projekt DEAL.

Conflict of Interests

The authors declare no conflict of interest.

Data Availability Statement

The data that support the findings of this study are openly available in KIT library at https://doi.org/10.5445/IR/1000151216.

Keywords: aluminum foil · AFM · surface roughness · microstructure · ionic liquid-based electrolyte

[1] C. Delmas, *Adv. Energy Mater.* **2018**, *8*, 1703137.
[2] K. Zhang, K. O. Kirlikovali, J. M. Suh, J. W. Choi, H. W. Jang, R. S. Varma, O. K. Farha, M. Shokouhimehr, *ACS Appl. Energ. Mater.* **2020**, *3*, 6019–6035.
[3] H. Yang, H. Li, J. Li, Z. Sun, K. He, H. M. Cheng, F. Li, *Angew. Chem. Int. Ed.* **2019**, *58*, 11978–11996.
[4] D. Yuan, J. Zhao, W. Manalastas, S. Kumar, M. Srinivasan, *Nano Mater. Sci.* **2020**, *2*, 248–263.
[5] G. A. Elia, K. Marquardt, K. Hoeppner, S. Fantini, R. Lin, E. Knipping, W. Peters, J. F. Drillet, S. Passerini, R. Hahn, *Adv. Mater.* **2016**, *28*, 7564–7579.
[6] J. Tu, W. L. Song, H. Lei, Z. Yu, L. L. Chen, M. Wang, S. Jiao, *Chem. Rev.* **2021**, *121*, 4903–4961.
[7] J. Liu, Z. Li, X. Huo, J. Li, *J. Power Sources* **2019**, *422*, 49–56.
[8] Y. Zhang, S. Liu, Y. Ji, J. Ma, H. Yu, *J. Adv. Mater.* **2018**, *30*, 1706310.
[9] J. Bitenc, U. Košir, A. Vizintin, N. Lindahl, A. Krajnc, K. Pirnat, I. Jerman, R. Dominko, *Energy Mater. Adv.* **2021**, 9793209.
[10] S. Guo, M. Liu, H. Yang, X. Feng, Y. Bai, C. Wu, *Green Energy & Environ.* **2023**, *8*, 883–892.
[11] X. Zhang, G. Zhang, S. Wang, S. Li, S. Jiao, *J. Mater. Chem. A* **2018**, *6*, 3084–3090.
[12] P. Moghimian, T. Poirié, M. Habibnejad-Korayem, J. A. Zavala, J. Kroeger, F. Marion, F. Larouche, *Addit. Manuf.* **2021**, *43*, 102017.
[13] C. Li, X. Zhang, W. He, *J. Mater. Sci. Mater. Electron.* **2018**, *29*, 14353–14370.
[14] H. Zhang, X. Jin, J. M. Lee, X. Wang, *ACS Nano* **2022**, *16*, 17572–17592.
[15] H. Wang, S. Gu, Y. Bai, S. Chen, N. Zhu, C. Wu, F. Wu, *J. Mater. Chem. A* **2015**, *3*, 22677–22686.
[16] X. Han, Y. Bai, R. Zhao, Y. Li, F. Wu, C. Wu, *Prog. Mater. Sci.* **2022**, *128*, 100960.
[17] T. Schoetz, C. Ponce de Leon, M. Ueda, A. Bund, *J. Electrochem. Soc.* **2017**, *164*, 3499–3502.
[18] G. A. Elia, I. Hasa, G. Greco, T. Diemant, K. Marquardt, K. Hoeppner, R. J. Behm, A. Hoell, S. Passerini, R. Hahn, *J. Mater. Chem. A* **2017**, *5*, 9682–9690.
[19] S. K. Das, S. Mahapatra, H. Lahan, *J. Mater. Chem. A* **2017**, *5*, 6347–6367.
[20] N. Zhu, K. Zhang, F. Wu, Y. Bai, C. Wu, *Energy Mater. Adv.* **2021**, *2021*, 204217.
[21] Y. Oh, G. Lee, Y. Tak, *ChemElectroChem* **2018**, *5*, 3348–3352.
[22] M. Chiku, H. Takeda, S. Matsumura, E. Higuchi, H. Inoue, *ACS Appl. Mater. Interfaces* **2015**, *7*, 24385–24389.
[23] L. Mei, J. Xu, Z. Wei, H. Liu, Y. Li, J. Ma, S. Dou, *Small* **2017**, *13*, 1701441.
[24] L. Geng, J. P. Scheifers, C. Fu, J. Zhang, B. P. T. Fokwa, J. Guo, *ACS Appl. Mater. Interfaces* **2017**, *9*, 21251–21257.
[25] Q. Zhou, Y. Zheng, D. Wang, Y. Lian, C. Ban, J. Zhao, H. Zhang, *Ceram. Int.* **2020**, *46*, 26454–26465.
[26] S. Divya, T. Nann, *ChemElectroChem* **2021**, *8*, 492–499.
[27] Z. A. Zafar, S. Imtiaz, R. Razaq, S. Ji, T. Huang, Z. Zhang, Y. Huang, J. A. Anderson, *J. Mater. Chem. A* **2017**, *5*, 5646–5660.
[28] Z. Zhou, N. Li, P. Wang, W. L. Song, S. Jiao, H. Chen, D. Fang, *J. Energy Chem.* **2020**, *42*, 17–26.
[29] K. V. Kravchyk, S. Wang, L. Piveteau, M. V. Kovalenko, *Chem. Mater.* **2017**, *29*, 4484–4492.
[30] X. Yu, B. Wang, D. Gong, Z. Xu, B. Lu, *J. Adv. Mater.* **2017**, *29*, 1604118.
[31] W. A. Appiah, H. Li, J. Lampkin, J. M. García-Lastra, *J. Power Sources* **2022**, *529*, 231254.
[32] Z. Liu, J. Wang, H. Ding, S. Chen, X. Yu, B. Lu, *ACS Nano* **2018**, *12*, 8456–8466.
[33] A. Ponrouch, J. Bitenc, R. Dominko, N. Lindahl, P. Johansson, M. R. Palacin, *Energy Storage Mater.* **2019**, *20*, 253–262.
[34] A. El Kharbachi, O. Zavorotynska, M. Latroche, F. Cuevas, V. Yartys, M. Fichtner, *J. Alloys Compd.* **2020**, *817*, 153261.
[35] K. N. Jung, H. S. Shin, M. S. Park, J. W. Lee, *ChemElectroChem* **2019**, *6*, 3842–3859.
[36] Z. Lin, M. Mao, J. Yue, B. Liu, C. Wu, L. Suo, Y. S. Hu, H. Li, X. Huang, L. Chen, *ACS Materials Lett.* **2020**, *2*, 808–813.
[37] Q. Zhao, J. Zheng, Y. Deng, L. Archer, *J. Mater. Chem. A* **2020**, *8*, 23231–23238.
[38] D. Ashkenazi, *Technol. Forecast. Soc. Change.* **2019**, *143*, 101–113.
[39] J. X. Johnson, C. A. Mcmillan, G. A. Keoleian, *J. Ind. Ecol.* **2013**, *17*, 700–711.
[40] S. Choi, H. Go, G. Lee, Y. Tak, *Phys. Chem. Chem. Phys.* **2017**, *19*, 8653–8656.
[41] J. Xu, J. Zhang, Z. Shi, *High Temp. Mater. Processes* **2013**, *32*, 367–373.
[42] H. Wang, H. Tan, X. Luo, H. Wang, T. Ma, M. Lv, X. Song, S. Jin, X. Chang, X. Li, *J. Mater. Chem. A* **2020**, *8*, 25649–25662.
[43] X. Chang, Z. Xie, Z. Liu, X. Zheng, J. Zheng, X. Li, *Energy Storage Mater.* **2020**, *25*, 93–99.
[44] G. A. Elia, K. V. Kravchyk, M. V. Kovalenko, J. Chacón, A. Holland, R. G. A. Wills, *J. Power Sources* **2021**, *481*, 228870.
[45] Y. Long, H. Li, M. Ye, Z. Chen, Z. Wang, Y. Tao, Z. Weng, S. Z. Qiao, Q. H. Yang, *Energy Storage Mater.* **2021**, *34*, 194–202.
[46] L. Gjønnes, *Wear.* **1996**, *192*, 216–227.
[47] E. H. Sunseri, R. Napolitano, K.-M. Ho, *Dendrite Orientation in Aluminum Magnesium Alloys* **2009**.
[48] L. C. Loaiza, N. Lindahl, P. Johansson, *J. Electrochem. Soc.* **2023**, *170*, 030512.
[49] G. Yue, S. Zhang, Y. Zhu, X. Lu, S. Li, Z. Li, *AIChE J.* **2009**, *55*, 783–796.
[50] X. Tu, J. Zhang, M. Zhang, Y. Cai, H. Lang, G. Tian, Y. Wang, *RSC Adv.* **2017**, *7*, 14790–14796.
[51] C. Didier, W. K. Pang, Z. Guo, S. Schmid, V. K. Peterson, *Chem. Mater.* **2020**, *32*, 2518–2531.
[52] H. T. Jeong, J. Jang, D. G. Lee, D. Lee, W. J. Kim, *J. Alloys Compd.* **2023**, *965*, 171279.
[53] B. Zhang, W. Zhang, H. Jin, J. Wan, *ChemistrySelect* **2023**, *8*, e202204575.
[54] J. L. Hutter, J. Bechhoefer, *Rev. Sci. Instrum.* **1993**, *64*, 1868–1873.
[55] G. A. Elia, N. A. Kyerematen, K. Marquardt, R. Hahn, *Batteries & Supercaps* **2019**, *2*, 83–90.

Manuscript received: July 7, 2023
Revised manuscript received: September 7, 2023
Accepted manuscript online: September 7, 2023
Version of record online: September 25, 2023